ACS APPLIED MATERIALS & INTERFACES

Research Article

Cite This: ACS Appl. Mater. Interfaces 2018, 10, 40951−40957

www.acsami.org

Magnetic Anisotropy Controlled by Distinct Interfacial Lattice Distortions at the $La_{1-x}Sr_xCoO_3/La_{2/3}Sr_{1/3}MnO_3$ Interfaces

Jine Zhang,[†,§,∥] Xiaobing Chen,[†,§,∥] Qinghua Zhang,[†,§] Furong Han,[†,§] Jing Zhang,[†,§] Hui Zhang,[†,§] Hongrui Zhang,[†,§] Hailin Huang,[†,§] Shaojin Qi,[†,§] Xi Yan,[†,§] Lin Gu,[†,§] Yuansha Chen,[†,§] Fengxia Hu,[†,§] Shishen Yan,[‡] Banggui Liu,[†,§] Baogen Shen,[†,§] and Jirong Sun*[,†,§]

[†]Beijing National Laboratory for Condensed Matter Physics & Institute of Physics, Chinese Academy of Sciences, Beijing 100190, People's Republic of China

[‡]Spintronics Institute, University of Jinan, Jinan 250022, Shandong, People's Republic of China

[§]School of Physical Sciences, University of Chinese Academy of Sciences, Beijing 100049, People's Republic of China

Supporting Information

ABSTRACT: Interface engineering is an important approach leading to multifunctional artificial materials. Although most of the previous works focused on the effects of the rotation/tilting of interfacial oxygen octahedron on perovskite multilayers, here, we report on a new kind of lattice distortion characterized by an off-center shift of the Mn ions within the MnO_6 oxygen octahedra at the interfaces of $La_{1-x}Sr_xCoO_3/La_{2/3}Sr_{1/3}MnO_3/La_{1-x}Sr_xCoO_3/LaAlO_3$ trilayers (x = 0−1/3), which drives the initially perpendicularly aligned magnetic axis of the $La_{2/3}Sr_{1/3}MnO_3$ (LSMO) film toward the in-plane direction, though the film is in a strongly compressive state. It is further found that the magnetic anisotropy considerably depends on the content of Sr in $La_{1-x}Sr_xCoO_3$, enhancing as x decreases. The maximal anisotropy constant at 10 K is $+2.5 \times 10^6$ erg/cm^3 for the trilayers with x = 0, whereas it is -1.5×10^5 erg/cm^3 for a bare LSMO film on $LaAlO_3$. On the basis of the analysis of X-ray absorption spectroscopy and the results of density functional theory calculations, we found that the off-center displacement of the Mn ions has caused a strong orbital reconstruction at interfaces, resulting in the anomalous spin orientation against magnetoelastic coupling.

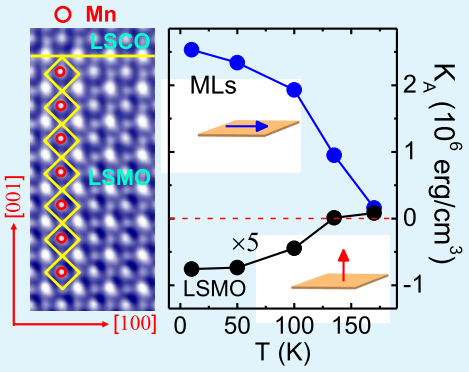

KEYWORDS: *trilayers, oxide interfaces, magnetic anisotropy, distinct interfacial lattice distortions, orbital reconstruction*

1. INTRODUCTION

Over the past decade, much effort has been devoted to the exploration of novel materials that can motivate new concepts of fundamental physics and practical applications, particularly those materials with a controllable spin texture/orientation, which play a central role in the investigation of some frontier areas including low-dimensional systems,[1,2] magnetic topological insulators,[3,4] magnetic vortices (skyrmions),[5,6] and the electric control of spin orientation.[7] ABO_3-type transition metal oxides are potential candidates for the designing of artificial materials with prerequisite spin texture/orientation due to their strongly coupled multiple degrees of freedom, which have resulted in a wide range of exotic physical properties.[8−11] Conventionally, magnetocrystalline anisotropy and magnetoelastic coupling are the basic mechanisms to determine spin orientation. Both characters have a close relation to strains that stem from lattice mismatch,[12] and thus are less controllable. As a distinct feature of perovskite oxides, interface engineering usually causes a rotation and/or tilting of the oxygen octahedron, resulting in a variation in magnetic anisotropy.[8−11] For example, by growing $La_{2/3}Sr_{1/3}MnO_3$ (LSMO) on $NdGaO_3$, which causes a tilting of the interfacial oxygen octahedron, Liao et al.[8] were able to rotate the easy magnetic axis of LSMO in the film plane by an angle of 90°; grouping perovskite LSMO with brownmillerite $LaCoO_{2.5}$, which causes an elongation and tilting of the oxygen octahedra, Zhang et al.[9] realized a switching of the easy axis from the in-plane (IP) to the out-of-plane (OP) direction for the LSMO layer. Accompanying the rotation and tilting of the BO_6 octahedra, orbital reconstruction takes place, modifying spin reorientation or spin texture.

Although most of the previous works focused on the effects of the BO_6 rotation/tilting, here, we report on a new kind of lattice distortion characterized by an off-center shift of the Mn ions within the MnO_6 oxygen octahedra at the interfaces of $La_{1-x}Sr_xCoO_3/LSMO/La_{1-x}Sr_xCoO_3$ (LSCO) trilayers grown on $LaAlO_3$ (LAO) (x = 0−1/3), which drives the easy magnetic axis of the LSMO film toward the IP direction, though the film is in a strongly compressive state that supports an OP anisotropy.[13,14] X-ray absorption spectroscopy (XAS)

Received: August 30, 2018
Accepted: October 19, 2018
Published: October 19, 2018

Downloaded via INST OF PHYSICS on December 10, 2018 at 12:25:09 (UTC).
See https://pubs.acs.org/sharingguidelines for options on how to legitimately share published articles.

© 2018 American Chemical Society

DOI: 10.1021/acsami.8b14981
ACS Appl. Mater. Interfaces 2018, 10, 40951−40957

analysis and density functional theory (DFT) calculations show that the off-center displacement of the Mn ions has caused a strong orbital reconstruction that supports the IP anisotropy. This work uncovers hidden aspects of lattice distortion at the interface between perovskite oxides, opening new avenues for the exploration of novel artificial materials of functionality.

2. EXPERIMENTAL SECTION

LSCO (7 nm)/LSMO (5 nm)/LSCO (7 nm) multilayer films with different chemical dopings (x = 0−0.33) in the LSCO layer were fabricated on (001)-oriented $LaAlO_3$ (LAO) single-crystal substrates (3 × 5 × 0.5 mm^3) by the pulsed laser deposition technique (KrF Excimer laser, wavelength = 248 nm). During the deposition process, the temperature of the substrate was kept at 700 °C (for LSMO) or 635 °C (for LSCO) and the oxygen atmosphere was fixed at 30 Pa. The fluence of the laser pulse was 2 J/cm^2, and the repetition rate was 2 Hz (KrF Excimer laser, wavelength = 248 nm). After deposition, the samples were cooled to room temperature at a rate of 10 °C/min in an oxygen atmosphere of 100 Pa. The film thickness was controlled by the number of laser pulses, which has been carefully calibrated by the small-angle X-ray reflectivity technique and a scanning transmission electron microscope (STEM).

The surface morphology of the multilayers was determined using an atomic force microscope (SPI 3800N; Seiko). The crystal structure of the samples was determined using a Bruker diffractometer equipped with thin-film accessories (D8 Discover, Cu Kα radiation). Lattice images of the films were recorded by a high-resolution scanning transmission electron microscope (STEM) with double C_S correctors (JEOL-ARM200F). Magnetic measurements were performed on a Quantum Design vibrating sample magnetometer (VSM-SQUID) in the temperature interval from 10 to 380 K and the magnetic field range up to 7 T.

The XAS spectrum of the Mn L-edge was collected at the beamline BL08U1A in Shanghai Synchrotron Radiation Facility, in the total electron yield mode. The spectra were measured for the two polarization directions of the linearly polarized X-rays, which are varied by rotating the X-ray incident angle, to 90° and 30° corresponding to the in-plane (E//a, I_{ab}) and out-of-plane (E//c, I_c) directions, respectively.[15] The spectral normalization was made by dividing the spectra by a factor such that the L_3 pre-edge and L_2 postedge have identical intensities for the two polarizations. After that, the pre-edge spectral region was set to zero and the peak at the L_3 edge was set to unity.[15,16] X-ray linear dichroism (XLD) is the difference between the two measurements ($I_{ab} - I_c$). The measurement temperature is 300 K.[16]

The DFT calculations were employed using a plane-wave basis set with the energy cutoff of 500 eV, and the projector augmented wave method[17] was implemented within the Vienna ab initio simulation package (VASP).[18,19] The spin-polarized Perdew−Burke−Ernzerhof modified for solids (PBEsol) functionals were used to describe the electron exchange and correlation effects.[20,21] The Brillouin zone was sampled with a 9 × 9 × 3 Monkhorst−Pack k-point mesh.[22] The DFT + U[23] approach was performed with U_{eff} = 3.0 and 3.3 eV for Mn and Co 3d orbitals, respectively,[24,25] to include the effect of strong correlation. To simulate the epitaxial growth on $LaAlO_3$, the in-plane lattice constants were fixed to 5.36 Å, which is the experimental lattice constant ($\sqrt{2}a$) of $LaAlO_3$. All of the atomic positions were optimized until the Hellmann−Feynman force on each atom was smaller than 0.01 eV $Å^{-1}$ and the absolute total energy difference between two successive loops was less than 10^{-5} eV. Moreover, the non-self-consistent DFT calculations with orientating the spins from the in-plane to the out-of-plane direction were performed to describe magnetocrystalline anisotropy.

3. RESULTS AND DISCUSSION

3.1. Structural Characteristics of the LSCO/LSMO/LSCO Trilayers. LSCO (7 nm)/LSMO (5 nm)/LSCO (7 nm) trilayers have been fabricated on (001)-oriented $LaAlO_3$ (LAO) substrates, where LSCO represents $La_{1-x}Sr_xCoO_3$ with x = 0, 0.05, 0.2, and 0.33 (Figure 1a). Here, the layer thickness

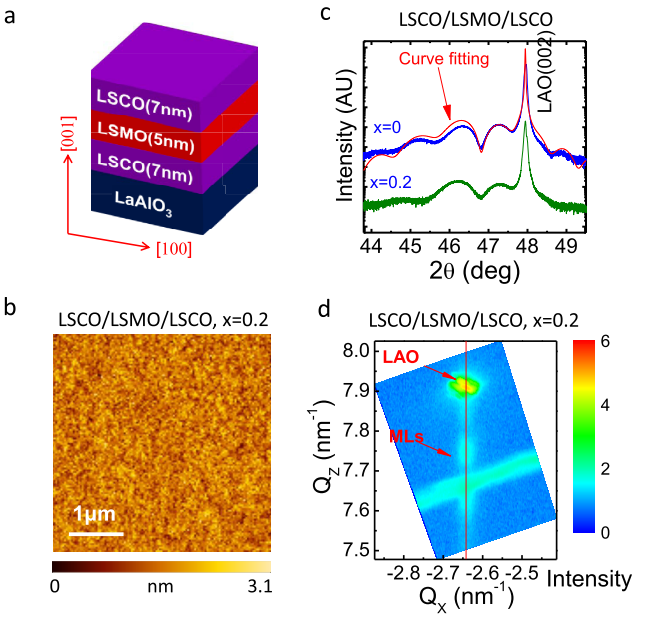

Figure 1. (a) Sketch of the multilayers grown on the LAO substrate. (b) Surface morphology of the LSCO/LSMO/LSCO trilayers (x = 0.2). The film is very flat with a root-mean-square roughness of ∼0.3 nm. (c) X-ray diffraction patterns for selected trilayers. Solid lines are results of curve fitting. (d) Reciprocal space mapping (RSM) of the ($\bar{1}03$) reflection of multilayers with x = 0.2. The vertical alignment for the reflections indicates the same IP lattice constant of the multilayers as that of the substrate. Here, "MLs" denotes multilayers.

was chosen such that it highlights the interfacial effect (Supporting Information, Figure S1). All multilayers are very flat, exhibiting the root-mean-square roughness of around 0.4 nm. This is an indication of a sharp interface in the multilayers. As an example, in Figure 1b, we show the morphology of LSCO/LSMO/LSCO with x = 0.2. The root-mean-square roughness is ∼0.3 nm, obtained over an area of 4 × 4 μm^2. Figure 1c illustrates the X-ray diffraction spectra of the LSCO/LSMO/LSCO multilayers with x = 0 and 0.2. A simulation of the diffraction/interference processes of the X-ray within three layers generates an output (red curve) that well mimics the experimental spectrum. The OP lattice parameter deduced from the curve fitting is 3.96 Å for LSMO and 3.86 Å for LSCO; the latter is essentially independent of the content of Sr in LSCO. The lattice constant is slightly larger than the bulk value (3.87 Å for LSMO and 3.83 Å for LSCO). Presumably, compressive IP strains exist in the films.

To determine the IP lattice parameters, we measured the reciprocal space mapping (RSM) of the ($\bar{1}03$) reflection. Figure 1d presents the typical results of the RSM of LSCO/LSMO/LSCO (x = 0.2). The most notable feature is the vertical alignment for the reflections of the multilayers and the LAO substrate. This is an indication of coherent growth of the multilayers on LAO, without lattice relaxation. This result supports the conclusion that the film is in an IP compressive state. Similar conclusions are applicable to other multilayers.

3.2. Magnetic Anisotropy of LCO/LSMO/LCO Trilayers. According to the preceding results, the LSMO layer in multilayers suffers from exactly the same lattice strains as its

DOI: 10.1021/acsami.8b14981
ACS Appl. Mater. Interfaces 2018, 10, 40951−40957

bare counterpart. However, we found that it is different from the bare LSMO in magnetic anisotropy, i.e., the easy magnetic axis prefers to lie in the film plane rather than along the OP direction as it usually does. To get a clear idea on this difference, we performed a comparative investigation of the bare LSMO film and the LSCO/LSMO/LSCO multilayers. Figure 2a,b illustrates temperature-dependent magnetization

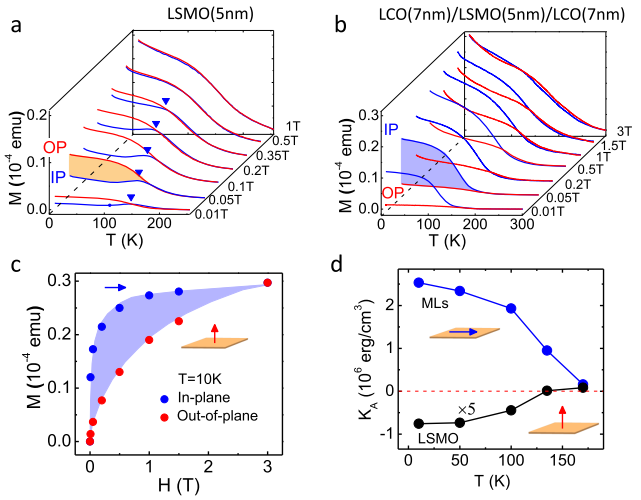

Figure 2. (a, b) Temperature-dependent magnetizations of the bare LSMO/LAO film and the LCO/LSMO/LCO multilayer films, respectively. Here, the data were acquired in the field-cooling mode with IP or OP applied fields. Orange and purple areas highlight the difference in the magnetic moments along the two measuring directions. Blue triangles in (a) mark the temperature for spin reorientation. (c) Magnetic moment as a function of applied fields, extracted from the data in (b) at T = 10 K. The shaded area corresponds to the energy required to orientate magnetic moment toward the OP direction. (d) Anisotropy constant as a function of temperature. Blue and black curves are the data of the LSMO film and the LCO/LSMO/LCO trilayers, respectively. Here, MLs denotes multilayers. The data of the LSMO/LAO single layer has been enlarged by 5 times for clarity.

($M-T$) of the bare LSMO film (5 nm) and the LSCO/LSMO/LSCO (x = 0) trilayers, respectively. For the LSMO film, as expected, the magnetization is considerably larger along the OP direction than that along the IP direction. This feature is especially obvious for the $M-T$ curves obtained in low fields. For high fields above 0.35 T, the magnetic anisotropy is overcome, and all magnetic moments now align along the field direction. The anisotropic constant, which is the energy required to align magnetic moment along the hard axis, is K_A = -1.5×10^5 erg/cm^3 at 10 K (the lowest temperature investigated). It is comparable to the previously reported values. The negative sign indicates a perpendicular easy axis. Here, the magnetic transition takes place in a wide temperature range. It is a general feature of an ultrathin film with strong lattice strains.

Cases are different for multilayers. The easy magnetic axis now switches from the OP to the IP direction. As shown in Figure 2b, the magnetic signals collected along the OP direction are very small when the magnetic field is lower than 0.2 T, without signatures of magnetic transition as the sample is cooled from 300 to 10 K. In contrast, a magnetic transition at 200 K can be clearly seen when applying the field along the IP direction, resulting in considerably enhanced magnetizations. Notably, the difference between the IP and OP $M-T$ curves remains significant under the field of 1.5 T. This implies that the IP magnetic anisotropy could be robust. Therefore, the LSMO layer sandwiched between two LCO layers shows an OP to IP spin reorientation, though the IP compressive strains support the perpendicular anisotropy. This is the most remarkable observation of this work and suggestive of the strong effect of the LCO layer on LSMO. Here, we would like to emphasize that the magnetic contribution of the multilayers solely comes from LSMO because LCO is nonmagnetic when grown on LAO.[26]

To get a quantitative description of magnetic anisotropy, a series of $M-H$ curves at different temperatures were extracted from the $M-T$ curves, as shown in Figure 2b. As an example, in Figure 2c, we show the $M-H$ curves at 10 K. Clearly, the magnetization shows different dependences on the magnetic field when the latter is applied along different directions. Along the IP direction, the magnetization increases rapidly with the magnetic field and reaches a saturation state above 0.5 T. In contrast, it keeps growing with the applied field until H = 3 T, when H is exerted perpendicular to the film plane. In principle, from the area encircled by the IP and OP $M-H$ curves, the magnetic anisotropic constant can be estimated. A direct calculation yields a K_A of $\sim 2.5 \times 10^6$ erg/cm^3 at 10 K. Compared to that of LSMO/LAO, notably, the K_A of LCO/LSMO/LCO is not only different in sign but also much greater in magnitude ($\sim 2.5 \times 10^6$ versus $\sim 1.5 \times 10^5$ erg/cm^3). It is even comparable to the K_A of the typical tensile LSMO/$SrTiO_3$ film ($\sim 4 \times 10^6$ erg/cm^3).[9] Obviously, the IP anisotropy of the multilayers is robust. This IP anisotropy is further evidenced by a direct measurement of magnetic loops with perpendicular and parallel fields (Supporting Information, Figure S2).

Similar phenomena are observed at other temperatures, though the detailed $M-H$ dependence varies with temperature. As a function of temperature, the magnetic anisotropic constant of LCO/LSMO/LCO is presented in Figure 2d. It is $\sim 2.5 \times 10^6$ erg/cm^3 at 10 K, decreasing slowly as the temperature increases from 10 to 100 K and falling rapidly upon further warming. The sign of the K_A remains positive over the whole temperature range investigated, implying the easy plane character of the LSMO layer in multilayers. For comparison, the anisotropic constant of the bare LSMO/LAO is also presented in Figure 2d.

3.3. Magnetic Anisotropy Tuned by the Sr Content in LSCO. Further investigations show that the magnetic anisotropy of the LSMO layer can be affected by not only LCO but also LSCO. Figure 3a shows the $M-T$ curves measured with an applied field of 0.05 T for the LSCO/LSMO/LSCO multilayers with the Sr content of x = 0–0.33. Let us focus our attention on the samples in the range of $0 \leq x \leq 0.2$, within which LSCO has no detectable magnetic contribution (Supporting Information, Figure S3). At first glance, the anisotropy is the strongest when x = 0 and slightly weakens as x increases from 0 to 0.2. To determine K_A, $M-T$ curves are also measured in different fields, and the corresponding $M-H$ relations were extracted from these $M-T$ curves (Supporting Information, Figure S4). On the basis of these data, the K_A-x relations are obtained. Figure 3b illustrates the variation of the anisotropy constant with the Sr content while fixing the temperature at 10 K. Although K_A exhibits a considerable decrease with increasing x, it is still as large as 2×10^6 erg/cm^3 for x = 0.2. For the sample of x =

DOI: 10.1021/acsami.8b14981
ACS Appl. Mater. Interfaces 2018, 10, 40951–40957

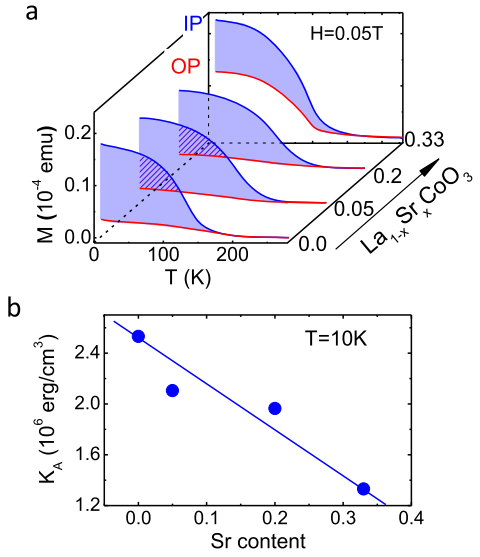

Figure 3. Effects of the Sr content in LSCO on magnetic behaviors of the trilayers. (a) Temperature-dependent magnetization of the LSCO/LSMO/LSCO trilayers, collected in the field-cooling mode with an IP or an OP applied field of 0.05 T. (b) Anisotropy constant as a function of Sr content in LSCO, displayed at a constant temperature of 10 K. Solid line is a guide for the eye.

0.33, the contribution of LSCO cannot be ignored. To make the data more complete, however, the corresponding result is also included in Figure 3b. Obviously, the IP anisotropy is a general feature of the LSMO layer sandwiched by LSCO, though LSMO is compressively strained. From first glance, K_A seems to obey a linear fitting curve even for the sample of x = 0.33 for which the magnetic contribution from LSCO is significant. A possible explanation could be that the magnetizations of the LSCO layers are similar when measured along the in-plane and out-of-plane directions and mostly counteract each other while calculating K_A.

3.4. Mechanism of Magnetic Anisotropy. It has been reported that the compressively strained LSMO film will exhibit a perpendicular magnetic anisotropy due to magnetoelastic coupling.[13,14] This is consistent with the observation in our bare LSMO/LAO films. Notably, the LSMO layer in multilayers is strained in exactly the same manner as the bare film. However, its easy magnetic axis changes dramatically, switching from the OP to the IP direction. A possible explanation is that the two LSCO neighbors have produced an effect on LSMO. To elucidate the mechanism for the IP anisotropy, the lattice structure of the multilayer is further studied. Figure 4a shows the typical high-angle annular dark-field (HAADF) image of LSCO/LSMO/LSCO (x = 0.2), recorded along the [001] zone using the scanning transmission electron microscope (STEM). Here, the brighter and fainter dots correspond to the La/Sr and Mn/Co atomic rows, respectively. At first glance, LSCO and LSMO grow coherently with each other, forming a perfect lattice structure. To get a quantitative characterization of the LSCO/LSMO interface, we performed a line profile analysis of the atomic contrast along the vertical Mn/Co columns. Figure 4d shows the intensity of the Mn/Co ions as a function of atomic position, obtained by averaging six sets of line profile data. Two features can be identified from Figure 4d. The first one is that the LSCO/LSMO interface is very sharp, without any signatures of cation

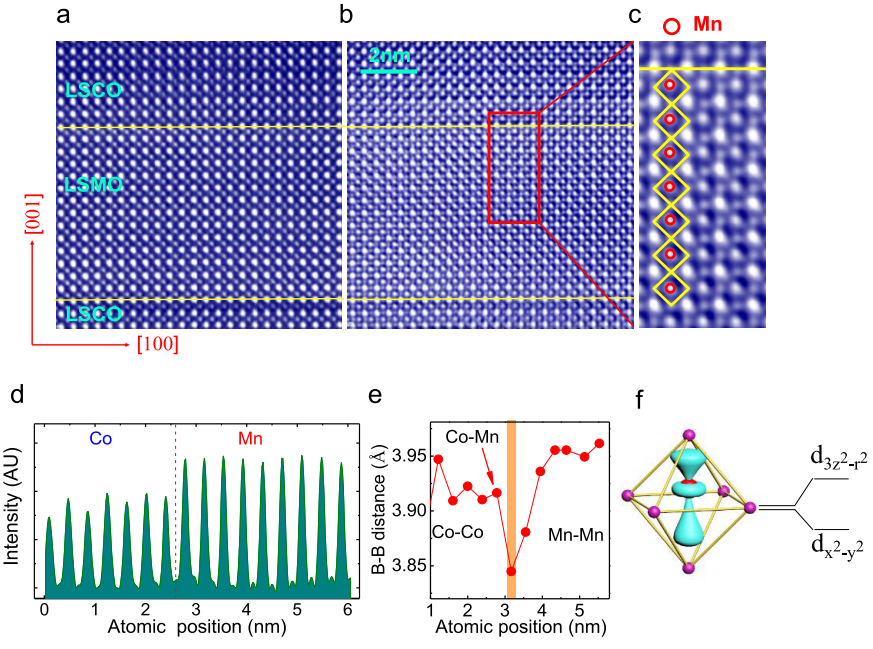

Figure 4. Lattice structure of the LSCO/LSMO/LSCO trilayers with x = 0.2. (a) Typical HAADF image of the cross section of the trilayers, recorded along the [001] zone. (b) Inverse annular bright-field (ABF) image taken from the same region as that for the HAADF image in (a). Yellow lines mark the LSCO/LSMO interface. (c) Enlarged ABF image highlighting the upper left shift of the Mn ion in the oxygen octahedron near the interface. The rhombus marks the oxygen octahedra and the red circle represents the Mn ions. (d) Spatial distribution of the Mn/Co ions, obtained by averaging six line profiles along the Mn/Co columns. The red dashed line represents the interface. The interface is sharp, without cation intermixing. (e) B−B distance as a function atomic position, obtained along vertical Mn/Co columns of the ABF image. The orange line marks the interface Mn−Mn distance. (f) Sketch of the distorted $d_{3z^2-r^2}$ orbital when the Mn ion moves toward the apical oxygen and the proposed energy levels for the $d_{3z^2-r^2}$ and $d_{x^2-y^2}$ orbitals.

DOI: 10.1021/acsami.8b14981
ACS Appl. Mater. Interfaces 2018, 10, 40951−40957

intermixing. The second one is that the Mn−Mn distance is smaller near the interface (Figure 4e), indicating an enhanced lattice distortion there.

To get further information about interface structure, the annular bright-field (ABF) image is simultaneously recorded. Figure 4b shows the inverse ABF image. In addition to the La/Sr and Mn/Co atoms, oxygen atoms can be clearly seen. This allows a quantitative analysis of the lattice structure, including the distortion of the oxygen octahedron and the displacement of the Mn/Co ions caged by the octahedra. At first glance, the position of the Mn/Co ions deviates from the center of the oxygen octahedron. As shown by the enlarged image in Figure 4c, relative to the oxygen octahedra, the Mn ions display an upper left shift, resulting in an electric polarity. This phenomenon is especially obvious near the LSCO/LSMO interface, fades out with the distance from the interface, and is invisible at six unit cells below the interface (Figure 4c). Fascinatingly, the oxygen octahedron is unaffected, without signatures of distortion or tilting. Its projection on the [100]−[001] plane forms a perfect rhombus. This is a new kind of lattice distortion that is not reported before at the interface between two perovskite oxides.

For a Mn ion in a compressive LSMO film, as well established, the preferentially occupied e_g orbital will be $d_{3z^2-r^2}$ because its energy level is lowered by the elongation of the MnO_6 octahedron along the OP direction. This is exactly the case taken place in the LSMO/LAO films.[15,27] When the Mn ions shift toward an oxygen ion in the octahedron, however, the $d_{3z^2-r^2}$ orbital will exhibit a higher energy level due to its enhanced overlap with O 2p orbitals (Figure 4f). As a result, it could be the $d_{x^2-y^2}$ rather than the $d_{3z^2-r^2}$ orbital that will be occupied, though LSMO is in a compressive state. This could be the main reason for the change in the magnetic anisotropy of the LSCO/LSMO/LSCO trilayers. In addition to the off-center displacement of the Mn ions, there are also many mechanisms for interfacial orbital reconstruction, including the effects of interface confinement, Mn−O−Co covalent bonding,[28] etc. These effects could also be the factors affecting the interfacial lattice distortions observed here. Obviously, further investigations in this regard are required.

To verify the interfacial orbital reconstruction, the spectra of X-ray absorption spectroscopy (XAS) of the Mn ions have been collected for a $[LSCO(4uc)/LSMO(4uc)]_5$ superlattice; here, x was set to be 0.33 for which a high-quality superlattice can be obtained. The measurement was performed at 300 K to avoid the interference of the ferromagnetic signal.[16] Figure 5 shows the normalized XAS spectra recorded with the optical polarizations parallel (E//a, I_{ab}) and perpendicular (E//c, I_c) to the film plane.[16,29] The L_2 peak in the energy range from 648 to 660 eV represents the occupancy of the $d_{x^2-y^2}$ or $d_{3z^2-r^2}$ orbital (blue or red curve, respectively).[16,29] Also shown in Figure 5 is the X-ray linear dichroism (XLD) spectrum defined by $I_{ab}-I_c$. The integration of the XLD spectrum from 648 to 660 eV gives a direct measure to empty Mn 3d states.[29] It outputs a negative value, indicating the preferred occupancy of the $d_{x^2-y^2}$ orbital.[16,29] This result is consistent with our preceding inference from the STEM results. At the same time, we also obtained the negative value of the standard LSMO/STO film with the IP magnetic anisotropy and the positive signal of the sample with the OP magnetic anisotropy (Supporting Information, Figure S5).

To get a further insight into the anomalous spin reorientation, density functional theory (DFT) calculations

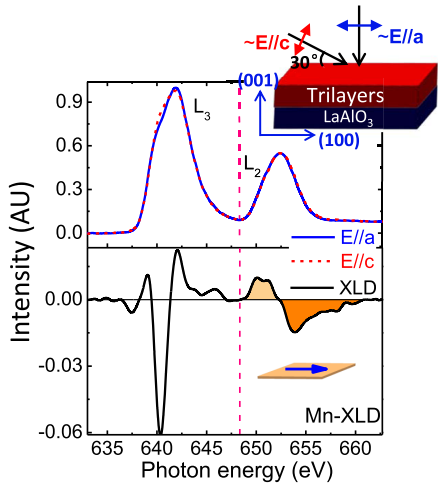

Figure 5. Normalized XAS spectra for the $[LSCO(4uc)/LSMO(4uc)]_5$ superlattices, measured with the polarized X-ray beam with different incident angles. The deduced XLD spectrum is also shown (black line). Its integration over the energy range from 648 to 660 eV (around the L_2 edge) gives a negative value, indicating IP magnetic anisotropy. Upper right corner: a sketch of the experimental setup for XAS measurements. The two incident angles of 90 and 30° for the X-ray beam correspond to the in-plane and out-of-plane polarizations, respectively.

were performed for the LSMO(3uc)/LCO(3uc) superlattice. Figure 6a shows the structural model for the DFT calculations.

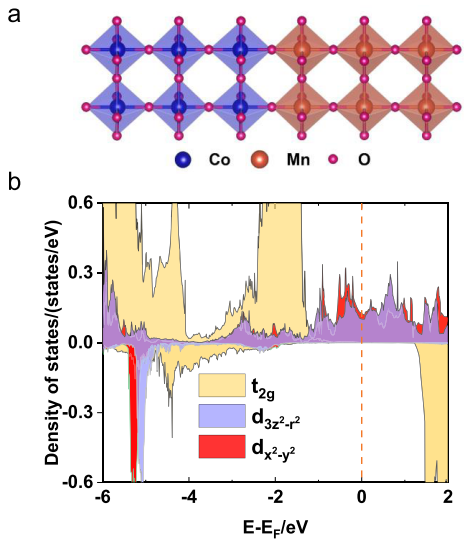

Figure 6. (a) Sketch of the LCO(3uc)/LSMO(3uc) superlattice for DFT calculations. La/Sr atoms have been removed for clarity. (b) Orbital-resolved partial density of Mn 3d states at the interfacial layer.

To explore the ground state, various magnetic states have been considered for the LSMO layer, including a ferromagnetic structure and A-, C-, and G-type antiferromagnetic structures. We finally found that LSMO is ferromagnetic and LCO is nonmagnetic. Figure 6b shows the orbital-resolved density of states for the LSMO(3uc)/LCO(3uc) superlattice. A direct calculation yields an occupancy ratio of 1.13:1 for the $d_{x^2-y^2}$ and $d_{3z^2-r^2}$ orbitals. This qualitatively agrees with the XLD result. This could be a consequence of structural distortion. We found that the length of the OP Mn−O−Mn bond decreases from 3.908 Å for the LSMO/LAO to 3.876 Å for the

DOI: 10.1021/acsami.8b14981
ACS Appl. Mater. Interfaces 2018, 10, 40951−40957

LSCO/LSMO superlattice. Moreover, we found that the easy axis lies in the film plane and the magnetic anisotropy energy, obtained by non-self-consistent DFT calculations, is ~1.2 × 10^6 erg/cm^3. This value is comparable to that of the experimental one (~2 × 10^6 erg/cm^3).

As well established, magnetocrystalline anisotropy and magnetoelastic coupling are the conventional mechanisms affecting spin orientation. However, they are the same for the LSCO-sandwiched LSMO layer and the bare LSMO film and therefore cannot be the mechanism for the anomalous IP anisotropy of the multilayers. According to the results of the STEM and XLD analyses and theoretical calculations, the main effect produced by interlayer coupling affects orbital occupancy. For the LSMO in multilayers, the $d_{x^2-y^2}$ orbital is preferentially occupied rather than $d_{3z^2-r^2}$ as for the bare LSMO/LAO film. In this case, the orbital momentum is finite in the IP direction and zero in the OP direction.[30] According to the Bruno model,[31,32] easy axis prefers to take the direction of the orbital momentum. This explains why the easy axis lies in the film plane for trilayers.

The decrease of the anisotropy constant with the incorporation of Sr could be ascribed to enhanced charge transfer. In general, charge transfer will take place across the LSCO/LSMO interface, from Mn ions to Co ions. This process has been detected across the $SrCoO_{2.5}$/LSMO interface.[28] This process will form an OP Co−O−Mn covalent bond, resulting in a preferential occupation of the $d_{3z^2-r^2}$ orbital. Obviously, charge transfer can produce an effect counteracting that of lattice distortion. This could be the reason for the reduction of K_A with x in LSCO/LSMO/LSCO.

By distorting the lattice structure at the LSMO/$LaCoO_{2.5}$ interface, in a previous work, Zhang et al.[9] obtained a strong OP anisotropy, which is expected to be IP-directed because the LSMO layer involved is in a tensile state. Here, we show how to turn the easy axis from the OP to IP direction via interface engineering. In general, the film with an IP anisotropy has the minimal magnetic leakage, which is widely used for magnetic shielding and magnetic circuit designing. Particularly, interface engineering has demonstrated its great potential in the exploration for artificial materials with novel functionality, which is characterized not only by controllable spin orientation but also by simultaneously existing electric polarity.

4. CONCLUSIONS

In summary, high-quality $La_{1-x}Sr_xCoO_3/La_{2/3}Sr_{1/3}MnO_3/La_{1-x}Sr_xCoO_3$ (x = 0−1/3) trilayers have been fabricated on $LaAlO_3$ substrates. A new kind of lattice distortion characterized by an off-center shift of the Mn ions within the MnO_6 oxygen octahedra has been observed in the atomic layers near the interface, which drives the initially perpendicularly aligned magnetic axis of the $La_{2/3}Sr_{1/3}MnO_3$ (LSMO) film toward the IP direction, though the film is in a highly compressive state. The anisotropy constant can be tuned in a wide range by incorporating different Sr contents into the $La_{1-x}Sr_xCoO_3$ layer. The maximum anisotropy constant at 10 K is as high as +2.5 × 10^6 erg/cm^3 for x = 0, which is in sharp contrast to the K_A of −1.5 × 10^5 erg/cm^3 of the bare $La_{2/3}Sr_{1/3}MnO_3/LaAlO_3$ layer. As evidenced by the analysis of X-ray absorption spectroscopy (XAS) and the results of density functional theory calculations, the off-center displacement of the Mn ions has caused an orbital reconstruction at interfaces, lifting the energy level of the $d_{3z^2-r^2}$ orbital with respect to that of $d_{x^2-y^2}$. This effect resulted in anomalous anisotropy. This work demonstrates the wide scope for the exploration of interfacial phases with unusual characteristics.

■ ASSOCIATED CONTENT

Supporting Information

The Supporting Information is available free of charge on the ACS Publications website at DOI: 10.1021/acsami.8b14981.

Magnetic loops with perpendicular and parallel fields of LSMO, $La_{0.8}Sr_{0.2}CoO_3$, LSCO/LSMO/LSCO (x = 0, 0.05, 0.2) films; thermomagnetic curves of the $La_{0.8}Sr_{0.2}CoO_3$ film and LSCO/LSMO/LSCO (x = 0, 0.05, 0.2, 0.33) trilayers; XAS and XLD spectra of the Mn $L_{2,3}$ edge of LSMO/STO film and $La_{0.67}Sr_{0.33}CoO_3$/LSMO multilayer films (PDF)

■ AUTHOR INFORMATION

Corresponding Author

*E-mail: jrsun@iphy.ac.cn.

ORCID

Jine Zhang: 0000-0001-7949-3239
Xiaobing Chen: 0000-0003-4327-1209
Lin Gu: 0000-0002-7504-031X
Banggui Liu: 0000-0002-6030-6680
Jirong Sun: 0000-0003-1238-8770

Author Contributions

‖J.Z. and X.C. contributed equally.

Notes

The authors declare no competing financial interest.

■ ACKNOWLEDGMENTS

We acknowledge beamline BL08U1A in Shanghai Synchrotron Radiation Facility (SSRF) for the XAS and XLD measurements. The calculations were performed in the Milky Way #2 supercomputer system at the National Supercomputer Center of Guangzhou, Guangzhou, China. This work has been supported by the National Basic Research of China (2016YFA0300701, 2017YFA0206300, and 2014CB920902), the National Natural Science Foundation of China (11520101002, 51590880, and 11674378), and the Key Program of the Chinese Academy of Sciences.

■ REFERENCES

(1) Wang, Z.; Tang, C.; Sachs, R.; Barlas, Y.; Shi, J. Proximity-Induced Ferromagnetism in Graphene Revealed by the Anomalous Hall Effect. *Phys. Rev. Lett.* **2015**, *114*, No. 016603.

(2) Lin, T.; Tang, C.; Alyahayaei, H. M.; Shi, J. Experimental Investigation of the Nature of the Magnetoresistance Effects in Pd-YIG Hybrid Structures. *Phys. Rev. Lett.* **2014**, *113*, No. 037203.

(3) Chang, C.-Z.; Zhang, J.; Feng, X.; Shen, J.; Zhang, Z.; Guo, M.; Li, K.; Ou, Y.; Wei, P.; Wang, L.-L.; Ji, Z.-Q.; Feng, Y.; Ji, S.; Chen, X.; Jia, J.; Dai, X.; Fang, Z.; Zhang, S.-C.; He, K.; Wang, Y.; Lu, L.; Ma, X.-C.; Xue, Q.-K. Experimental Observation of the Quantum Anomalous Hall Effect in a Magnetic Topological Insulator. *Science* **2013**, *340*, 167−170.

(4) Chang, C.-Z.; Zhang, J.; Liu, M.; Zhang, Z.; Feng, X.; Li, K.; Wang, L.-L.; Chen, X.; Dai, X.; Fang, Z.; Qi, X.-L.; Zhang, S.-C.; Wang, Y.; He, K.; Ma, X.-C.; Xue, Q.-K. Thin Films of Magnetically Doped Topological Insulator with Carrier-Independent Long-Range Ferromagnetic Order. *Adv. Mater.* **2013**, *25*, 1065−1070.

(5) Huang, S. X.; Chien, C. L. Extended Skyrmion Phase in Epitaxial FeGe(111) Thin Films. *Phys. Rev. Lett.* **2012**, *108*, No. 267201.

DOI: 10.1021/acsami.8b14981
ACS Appl. Mater. Interfaces 2018, 10, 40951−40957

(6) Rößler, U. K.; Bogdanov, A. N.; Pfleiderer, C. Spontaneous skyrmion ground states in magnetic metals. *Nature* **2006**, *442*, 797−801.
(7) Zhai, K.; Wu, Y.; Shen, S.; Tian, W.; Cao, H.; Chai, Y.; Chakoumakos, B. C.; Shang, D.; Yan, L.; Wang, F.; Sun, Y. Giant magnetoelectric effects achieved by tuning spin cone symmetry in Y-type hexaferrites. *Nat. Commun.* **2017**, No. 519.
(8) Liao, Z.; Huijben, M.; Zhong, Z.; Gauquelin, N.; Macke, S.; Green, R. J.; Van Aert, S.; Verbeeck, J.; Van Tendeloo, G.; Held, K.; Sawatzky, G. A.; Koster, G.; Rijnders, G. Controlled lateral anisotropy in correlated manganite heterostructures by interface-engineered oxygen octahedral coupling. *Nat. Mater.* **2016**, *15*, 425−431.
(9) Zhang, J.; Zhong, Z.; Guan, X.; Shen, X.; Zhang, J.; Han, F.; Zhang, H.; Zhang, H.; Yan, X.; Zhang, Q.; Gu, L.; Hu, F.; Yu, R.; Shen, B.; Sun, J. Symmetry mismatch-driven perpendicular magnetic anisotropy for perovskite/brownmillerite heterostructures. *Nat. Commun.* **2018**, *9*, No. 1923.
(10) Yi, D.; Flint, C. L.; Balakrishnan, P. P.; Mahalingam, K.; Urwin, B.; Vailionis, A.; N'Diaye, A. T.; Shafer, P.; Arenholz, E.; Choi, Y.; Stone, K. H.; Chu, J.-H.; Howe, B. M.; Liu, J.; Fisher, I. R.; Suzuki, Y. Tuning Perpendicular Magnetic Anisotropy by Oxygen Octahedral Rotations in $(La_{1-x}Sr_xMnO_3)/(SrIrO_3)$ Superlattices. *Phys. Rev. Lett.* **2017**, *119*, No. 077201.
(11) Kan, D.; Aso, R.; Sato, R.; Haruta, M.; Kurata, H.; Shimakawa, Y. Tuning magnetic anisotropy by interfacially engineering the oxygen coordination environment in a transition metal oxide. *Nat. Mater.* **2016**, *15*, 432−437.
(12) Chen, Y. B.; Sun, H. P.; Katz, M. B.; Pan, X. Q.; Choi, K. J.; Jang, H. W.; Eom, C. B. Interface structure and strain relaxation in $BaTiO_3$ thin films grown on $GdScO_3$ and $DyScO_3$ substrates with buried coherent $SrRuO_3$ layer. *Appl. Phys. Lett.* **2007**, *91*, No. 252906.
(13) Tsui, F.; Smoak, M. C.; Nath, T. K.; Eom, C. B. Strain-dependent magnetic phase diagram of epitaxial $La_{0.67}Sr_{0.33}MnO_3$ thin films. *Appl. Phys. Lett.* **2000**, *76*, 2421−2423.
(14) Dho, J.; Kim, Y. N.; Hwang, Y. S.; Kim, J. C.; Hur, N. H. Strain-induced magnetic stripe domains in $La_{0.7}Sr_{0.3}MnO_3$ thin films. *Appl. Phys. Lett.* **2003**, *82*, 1434−1436.
(15) Cui, B.; Song, C.; Li, F.; Wang, G. Y.; Mao, H. J.; Peng, J. J.; Zeng, F.; Pan, F. Tuning the entanglement between orbital reconstruction and charge transfer at a film surface. *Sci. Rep.* **2014**, *4*, No. 4206.
(16) Pesquera, D.; Herranz, G.; Barla, A.; Pellegrin, E.; Bondino, F.; Magnano, E.; Sánchez, F. S. A.; Fontcuberta, J. Surface symmetry-breaking and strain effects on orbital occupancy in transition metal perovskite epitaxial films. *Nat. Commun.* **2012**, *3*, No. 1189.
(17) Blöchl, P. E. Projector augmented-wave method. *Phys. Rev. B* **1994**, *50*, No. 17953.
(18) Kresse, G.; Hafner, J. *Ab initio* molecular dynamics for liquid metals. *Phys. Rev. B* **1993**, *47*, No. 558.
(19) Kresse, G.; Hafner, J. *Ab initio* molecular-dynamics simulation of the liquid-metal -amorphous-semiconductor transition in germanium. *Phys. Rev. B* **1994**, *49*, No. 14251.
(20) Perdew, J. P.; Burke, K.; Ernzerhof, M. Generalized Gradient Approximation Made Simple. *Phys. Rev. Lett.* **1996**, *77*, No. 3865.
(21) Perdew, J. P.; Ruzsinszky, A.; Csonka, G. I.; Vydrov, O. A.; Scuseria, G. E.; Constantin, L. A.; Zhou, X.; Burke, K. Restoring the Density-Gradient Expansion for Exchange in Solids and Surfaces. *Phys. Rev. Lett.* **2008**, *100*, No. 136406.
(22) Anisimov, V. I.; Zaanen, J.; Anderson, O. K. Band theory and Mott insulators: Hubbard *U* instead of Stoner *I*. *Phys. Rev. B* **1991**, *44*, No. 943.
(23) Monkhorst, H. J.; Pack, J. D. Special Points for Brillonin-zone Integrations. *Phys. Rev. B* **1976**, *13*, No. 5188.
(24) Cai, Z.; Kuru, Y.; Han, J. W.; Chen, Y.; Yildiz, B. Surface Electronic Structure Transitions at High Temperature on Perovskite Oxides: The Case of Strained $La_{0.8}Sr_{0.2}CoO_3$ Thin Films. *J. Am. Chem. Soc.* **2011**, *133*, 17696−17704.
(25) Zhang, Q.; Dong, S.; Wang, B. L.; Yunoki, S. Strain-engineered Magnetic Order in $(LaMnO_3)_n/(SrMnO_3)_{2n}$ Superlattices. *Phys. Rev. B* **2012**, *86*, No. 094403.
(26) Yang, H. W.; Zhang, H. R.; Li, Y.; Wang, S. F.; Shen, X.; Lan, Q. Q.; Meng, S.; Yu, R. C.; Shen, B. G.; Sun, J. R. Anomalous magnetism in strained $La_{1-x}Sr_xCoO_3$ epitaxial films $(0 \leq x \leq 0.5)$. *Sci. Rep.* **2014**, *4*, No. 6206.
(27) Aruta, C.; Ghiringhelli, G.; Bisogni, V.; Braicovich, L.; Brookes, N. B.; Tebano, A.; Balestrino, G. Orbital occupation, atomic moments, and magnetic ordering at interfaces of manganite thin films. *Phys. Rev. B* **2009**, *80*, No. 014431.
(28) Cui, B.; Li, F.; Song, C.; Peng, J. J.; Saleem, M. S.; Gu, Y. D.; Li, S. N.; Wang, K. L.; Pan, F. Insight into the antiferromagnetic structure manipulated by electronic reconstruction. *Phys. Rev. B* **2016**, *94*, No. 134403.
(29) Huijben, M.; Martin, L. W.; Chu, Y. H.; Holcomb, M. B.; Yu, P.; Rijnders, G.; Blank, D. H. A.; Ramesh, R. Critical thickness and orbital ordering in ultrathin $La_{0.7}Sr_{0.3}MnO_3$ films. *Phys. Rev. B* **2008**, *78*, No. 094413.
(30) Stöhr, J.; Siegmann, H. C. *Magnetism: From Fundamentals to Nanoscale Dynamics*; Springer: Heidelberg, 2006; pp 305−308.
(31) Bruno, P. Tight-binding approach to the orbital magnetic moment and magnetocrystalline anisotropy of transition-metal monolayers. *Phys. Rev. B* **1989**, *39*, No. 865.
(32) Bruno, P. Magnetismus Von Festkörpern und Grenzflächen. In *Ferienkurse des Forschungszentrums Jülich*; KFA: Jülich, Germany, 1993; Chapter 24, p 1.

DOI: 10.1021/acsami.8b14981
ACS Appl. Mater. Interfaces 2018, 10, 40951−40957